

# Astro2020 APC White Paper

## CMB Spectral Distortions: Status and Prospects

**Primary thematic area:** Cosmology and Fundamental Physics

**Secondary thematic area:** Galaxy Evolution

**Corresponding author email:** alan.j.kogut@nasa.gov

A. Kogut<sup>1</sup>, M. H. Abitbol<sup>2</sup>, J. Chluba<sup>3</sup>, J. Delabrouille<sup>4,5</sup>, D. Fixsen<sup>6</sup>, J. C. Hill<sup>7,8</sup>, S. P. Patil<sup>9</sup>,  
and A. Rotti<sup>3</sup>

<sup>1</sup> NASA/GSFC, Mail Code: 665, Greenbelt, MD 20771, USA

<sup>2</sup> University of Oxford, Denys Wilkinson Building, Keble Road, Oxford, OX1 3RH, UK

<sup>3</sup> Jodrell Bank Centre for Astrophysics, School of Physics and Astronomy, The University of Manchester, Manchester M13 9PL, U.K.

<sup>4</sup> Laboratoire Astroparticule et Cosmologie (APC), CNRS/IN2P3, 10, rue Alice Domon et Léonie Duquet, 75205 Paris Cedex 13, France

<sup>5</sup> Département d'Astrophysique, CEA Saclay DSM/Irfu, 91191 Gif-sur-Yvette, France

<sup>6</sup> Department of Astronomy, University of Maryland, College Park, MD 20742-2421, USA

<sup>7</sup> Institute for Advanced Study, Princeton, NJ 08540, USA

<sup>8</sup> Center for Computational Astrophysics, Flatiron Institute, 162 5th Avenue, New York, NY 10010, USA

<sup>9</sup> Niels Bohr International Academy and Discovery Center, Blegdamsvej 17, 2100 Copenhagen, Denmark

Submitted in response to the Activity and Project APC call  
Decadal Survey of Astronomy and Astrophysics 2020

### Endorsers

---

Yacine Ali-Haïmoud	Physics Department, New York University
Mustafa A. Amin	Dept. of Physics and Astronomy, Rice University
Nicola Bartolo	Dipartimento di Fisica e Astronomia, Università degli Studi di Padova
Ritoban Basu Thakur	California Institute of Technology
Ido Ben-Dayan	Ariel University
Boris Bolliet	Jodrell Bank Centre for Astrophysics, University of Manchester
J. Richard Bond	Canadian Institute for Theoretical Astrophysics, University of Toronto
Francois R. Bouchet	Institut d'Astrophysique de Paris, CNRS & Sorbonne Université
Cliff Burgess	McMaster University and Perimeter Institute
Carlo Burigana	Istituto Nazionale di Astrofisica (INAF), Istituto di Radioastronomia
Chris Byrnes	Department of Physics and Astronomy, University of Sussex
Giovanni Cabass	Max-Planck-Institut für Astrophysik
David T. Chuss	Department of Physics Villanova University
Sebastien Clesse	Cosmology, Universe and Relativity at Louvain (CURL), University of Louvain
Liang Dai	Institute For Advanced Study, Princeton NJ
Vincent Desjacques	Physics Department and Asher Space Science Institute
Gianfranco De Zotti	Istituto Nazionale di Astrofisica (INAF)-Osservatorio Astronomico di Padova
Emanuela Dimastrogiovanni	School of Physics, The University of New South Wales
Eleonora Di Valentino	Jodrell Bank Center for Astrophysics, University of Manchester
Olivier Dore	California Institute of Technology
Jo Dunkley	Physics Department, Princeton University
Ruth Durrer	Département de Physique Théorique, Université de Genève
Cora Dvorkin	Department of Physics, Harvard University
H. K. Eriksen	Institute of Theoretical Astrophysics, University of Oslo

---

Continued on next page

---

**Endorsers (continued)**

---

Tom Essinger-Hileman	NASA Goddard Space Flight Center
Matteo Fasiello	Institute of Cosmology and Gravitation, University of Portsmouth
Fabio Finelli	Instituto Nazionale di Astrofisica (INAF)
Raphael Flauger	Department of Physics, UC San Diego
Juan García-Bellido	Instituto de Física Teórica, Universidad Autónoma de Madrid
Massimo Gervasi	University of Milano Bicocca
Daniel Grin	Haverford College
Diego Herranz	Instituto de Física de Cantabria (CSIC-UC)
Donghui Jeong	Department of Astronomy and Astrophysics, The Pennsylvania State University
Bradley R. Johnson	Department of Physics, Columbia University
Rishi Khatri	Department of Theoretical Physics, Tata Institute of Fundamental Research
Kazunori Kohri	KEK
Kerstin E. Kunze	University of Salamanca
John C. Mather	NASA Goddard Space Flight Center
Sabino Matarrese	Dipartimento di Fisica e Astronomia, Università degli Studi di Padova
Joel Meyers	Department of Physics, Southern Methodist University
Nareg Mirzaturyan	Department of Physics and Astronomy, University of Southern California
Suvodip Mukherjee	Institut d'Astrophysique de Paris
Moritz Münchmeyer	Perimeter Institute for Theoretical Physics
Tomohiro Nakama	Institute for Advanced Study, The Hong Kong University of Science and Technology
P.Naselsky	Niels Bohr Institute
Federico Nati	Department of Physics, University of Milano - Bicocca
Elena Orlando	Stanford University
Enrico Pajer	DAMTP, University of Cambridge
Elena Pierpaoli	University of Southern California
Levon Pogosian	Department of Physics, Simon Fraser University
Vivian Poulin	CNRS & Université de Montpellier
Andrea Ravenni	Jodrell Bank Centre for Astrophysics, The University of Manchester
Christian L. Reichardt	School of Physics, University of Melbourne
Mathieu Remazeilles	Jodrell Bank Centre for Astrophysics, The University of Manchester
Graca Rocha	JPL / California Institute of Technology
Karwan Rostem	NASA Goddard Space Flight Center
Jose Alberto Rubiño-Martin	Instituto de Astrofísica de Canarias
Giorgio Savini	Dept. Physics and Astronomy, University College London
Douglas Scott	University of British Columbia
Pasquale D. Serpico	LAPTh, Univ. Grenoble Alpes
A. A. Starobinsky	L. D. Landau Institute for Theoretical Physics
Tarun Souradeep	Inter-University Centre for Astronomy and Astrophysics (IUCAA)
Ravi Subrahmanyan	Raman Research Institute,
Andrea Tartari	Istituto Nazionale di Fisica Nucleare
Tiziana Trombetti	CNR, ISMAR Bologna
I. K. Wehus	Institute of Theoretical Astrophysics, University of Oslo
Siavash Yasini	University of Southern California

---

## Executive Summary

Departures of the energy spectrum of the cosmic microwave background (CMB) from a perfect blackbody probe a fundamental property of the universe – its thermal history. Current upper limits, dating back some 25 years, limit such spectral distortions to 50 parts per million and provide a foundation for the Hot Big Bang model of the early universe. Modern upgrades to the 1980’s-era technology behind these limits enable three orders of magnitude or greater improvement in sensitivity. The standard cosmological model provides compelling targets at this sensitivity, spanning cosmic history from the decay of primordial density perturbations to the role of baryonic feedback in structure formation. Fully utilizing this sensitivity requires concurrent improvements in our understanding of competing astrophysical foregrounds. We outline a program using proven technologies capable of detecting the minimal predicted distortions even for worst-case foreground scenarios.

## 1. Science Goals

The cosmic microwave background (CMB) provides powerful tests for cosmology. A remnant from the early universe, today it dominates the sky at millimeter wavelengths. Its near-perfect blackbody spectrum provides compelling evidence for a hot, dense phase at very early times. However, deviations from a blackbody (so-called spectral distortions) are expected and encode information over the entire thermal history of the universe. As discussed in [1], spectral distortions result from out-of-equilibrium energy exchange between matter and radiation. After energy release into the plasma, Compton scattering of CMB photons by the electron gas distorts the CMB spectrum as photons are scattered to higher energies. Once photon-creating processes become negligible at redshift  $z < 2 \times 10^6$ , the spectrum is unable to evolve back to a (hotter) blackbody, locking in a distortion whose amplitude and spectral shape depend on the epoch, duration, and amplitude of the energy release. Optically thin scattering ( $z < 10^4$ ) creates a Compton  $y$ -distortion characterized by the parameter  $y \propto \int n_e(T_e - T_\gamma)dz$  proportional to the integrated electron pressure. Optically thick scattering ( $z > 3 \times 10^5$ ) yields the equilibrium Bose-Einstein spectrum, characterized by the chemical potential  $\mu = 1.4\Delta E/E$  proportional to the fractional energy release relative to the energy in the CMB bath. Energy release at  $10^4 < z < 3 \times 10^5$  produces an intermediate spectrum,

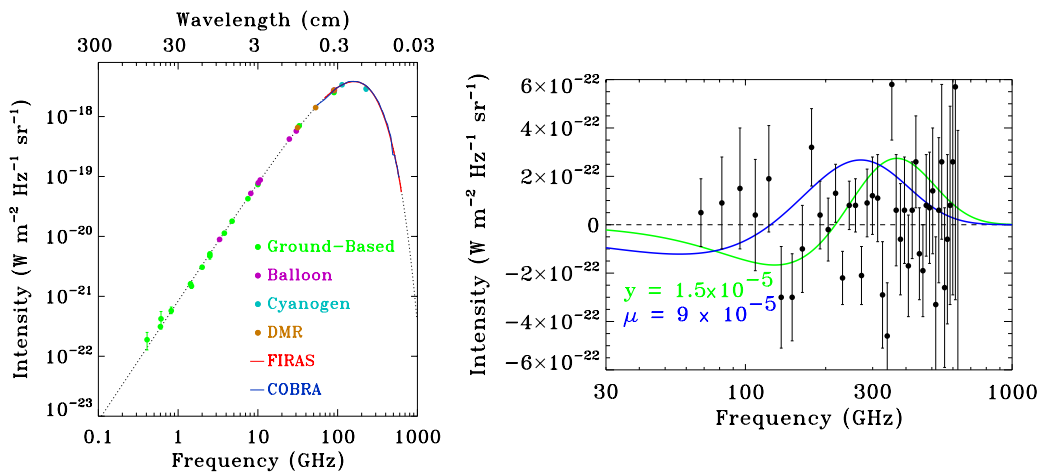


Figure 1: CMB intensity spectrum and spectral distortions. (Left) The absolute intensity of the CMB follows a blackbody Planck distribution. (Right)  $y$  and  $\mu$  spectral distortions at the FIRAS 95% confidence upper limit.

encoding additional time-dependent information [2–6]. Additional rich distortion shapes can be created by photon-injection processes and interactions with high-energy, non-thermal particles [7–9].

Figure 1 shows the CMB blackbody spectrum and spectral distortions. Current upper limits to spectral distortions date to the seminal Far Infrared Absolute Spectrophotometer (FIRAS) measurements in the 1990’s. FIRAS limits spectral distortions to  $|y| < 15 \times 10^{-6}$  and  $|\mu| < 9 \times 10^{-5}$  corresponding to fractional distortion  $\Delta I/I < 50$  parts per million [10]. Observational progress since FIRAS has been limited. Measurements in the low-frequency Rayleigh-Jeans tail from ground-based and balloon platforms confirmed that the spectrum remains consistent with a blackbody to 0.1% at these frequencies, but did not improve FIRAS constraints on spectral distortions [11–14].

**Straightforward upgrades to the FIRAS instrument design would enable breakthrough science.** FIRAS was not background limited; its sensitivity was set instead by phonon noise from its 1.4 K detector. Modern detectors operating at 0.1 K have demonstrated phonon noise well below the intrinsic limit set by photon arrival statistics. Most of the usable FIRAS data came from a single detector, whose operational lifetime of 10 months ended when the liquid helium ran out. Combining a modest number of background-limited detectors with the longer observing times made possible using mechanical cryocoolers would improve sensitivity by three orders of magnitude. **The sky cannot be black at this level: new measurements provide compelling tests of the standard cosmological model and open a vast discovery space for new physics beyond this model.** Examples include spectral distortions induced by the decay of long-lived dark matter particles (with lifetimes between  $t \approx 10^6 - 10^{12}$  s), dark matter-standard model particle interactions, gravitino decays, axion-photon conversion, as well as distortions produced by cosmic strings and primordial magnetic fields. Spectral distortions are also a powerful probe of primordial non-Gaussianity and enhanced (or reduced) power in the primordial power spectrum at scales far beyond those accessed by CMB anisotropies, such as those recently favored by inflationary scenarios that produce LIGO mass primordial black holes [1]. In addition to this, the cosmological standard model is expected to produce its own “floor” of spectral distortions through various mechanisms such as the interaction of CMB photons with hot electrons during reionization and large-scale structure formation, the cosmological recombination process, non-equilibrium processes in the pre-recombination hydrogen and helium plasma, and the acoustic dissipation of small-scale primordial perturbations within the standard cosmological scenario [15,16]. ASTRO2020 science response 205 [1] summarizes the science from spectral distortions. In what follows, we lay out a road map for observing CMB spectral distortions at the sensitivity required to probe this physics.

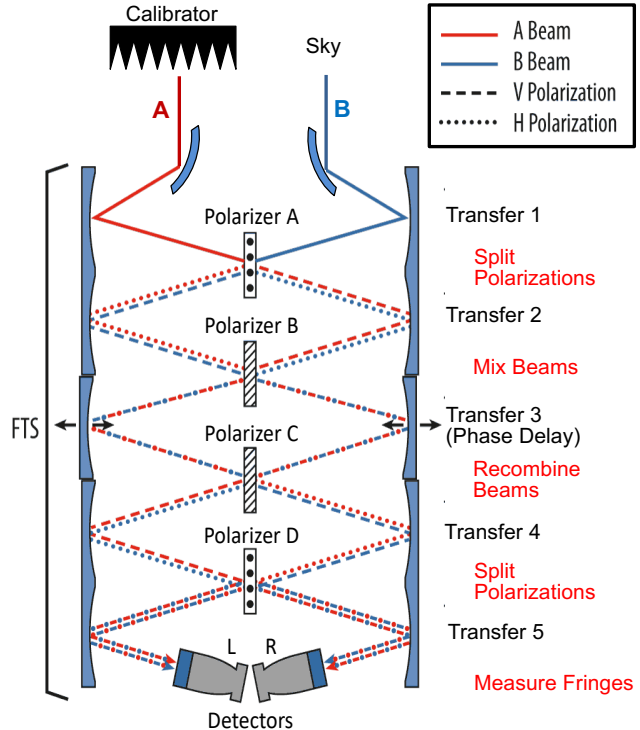


Figure 2: Optical signal path for a fully symmetric Fourier Transform Spectrometer (FTS).

## 2. Measurement Fundamentals

Fourier transform spectroscopy is ideally suited to search for CMB spectral distortions. Figure 2 shows the concept. Two input ports accept light from co-pointed beams on the sky. A set of five transfer mirror pairs, each imaging the previous mirror to the following one, shuttles the radiation through a series of polarizing wire grids. Polarizer A transmits vertical polarization and reflects horizontal polarization, separating each beam into orthogonal polarization states. A second polarizer (B) with wires oriented  $45^\circ$  relative to grid A mixes the polarization states. A Mirror Transport Mechanism (MTM) moves the central pair of transfer mirrors to inject an optical phase delay. The phase-delayed beams re-combine (interfere) at Polarizer C. Polarizer D (oriented the same as A) splits the beams again and routes them to a set of multi-moded concentrator feed horns. Each feed contains a pair of identical bolometers, each sensitive to a single linear polarization but mounted at  $90^\circ$  to each other to measure orthogonal polarization states. As the MTM sweeps back and forth, the recombined beams interfere to create a fringe amplitude dependent on the optical phase delay between the two beams. Let  $\vec{E} = E_x\hat{x} + E_y\hat{y}$  represent the electric field incident from the sky. The power at the detectors as a function of frequency  $\omega$  and mirror position  $z$  may be written

$$\begin{aligned}
 P_{Lx} &= 1/2 \int \{ (E_{Ax}^2 + E_{By}^2) + (E_{Ax}^2 - E_{By}^2) \cos(4z\omega/c) \} d\omega , \\
 P_{Ly} &= 1/2 \int \{ (E_{Ay}^2 + E_{Bx}^2) + (E_{Ay}^2 - E_{Bx}^2) \cos(4z\omega/c) \} d\omega , \\
 P_{Rx} &= 1/2 \int \{ (E_{Ay}^2 + E_{Bx}^2) + (E_{Bx}^2 - E_{Ay}^2) \cos(4z\omega/c) \} d\omega , \\
 P_{Ry} &= 1/2 \int \{ (E_{Ax}^2 + E_{By}^2) + (E_{By}^2 - E_{Ax}^2) \cos(4z\omega/c) \} d\omega ,
 \end{aligned} \tag{1}$$

where L and R refer to the detectors in the left and right concentrators while A and B refer to the two input beams (Fig 2).

We may sample the fringe pattern  $P(z)$  measured at each detector at a set of  $N_s$  mirror positions to recover the frequency spectrum of the incident radiation. Let  $S_\nu$  represent the frequency-dependent sky signal and  $S_k$  represent the amplitude of the sampled fringe pattern. The two are related by a Fourier transform,

$$S_k = \int S_\nu \exp\left(\frac{2\pi i z_k \nu}{c}\right) d\nu , \quad S_\nu = \sum_{k=0}^{N_s-1} W_k S_k \exp\left(\frac{2\pi i \nu k Z}{c N_s}\right) , \tag{2}$$

where  $z_k$  is the phase delay for fringe sample  $k$ ,  $W_k$  is the apodization weight, and  $k$  labels the synthesized frequency channels. As the mirror moves, we obtain  $N_s$  detector samples over an optical path length  $\pm Z$ . The Fourier transform of the sampled fringe pattern returns the sky signal at sampled frequencies  $n \times c/(2Z)$  where  $n = 0, 1, 2, \dots, N_s/2$ . The maximum path length (optical stroke) thus determines the width of the frequency bins in the synthesized spectra, while the number of detector samples within each optical stroke determines the number of frequency bins and thus the highest sampled frequency.

The noise equivalent power (NEP) of photon noise in a single linear polarization is determined by

$$\text{NEP}_{\text{photon}}^2 = \frac{2A\Omega}{c^2} \frac{(kT)^5}{h^3} \int \alpha \epsilon f \frac{x^4}{e^x - 1} \left(1 + \frac{\alpha \epsilon f}{e^x - 1}\right) dx , \tag{3}$$

where  $A$  is the detector area,  $\Omega$  is the detector solid angle,  $\alpha$  is detector absorptivity,  $T$  is the physical temperature of the source,  $\epsilon$  is the emissivity of the source, and  $f$  is the power

transmission through the optics [17]. For a fixed integration time,  $\tau$ , the detected noise is then simply

$$\delta P = \frac{\text{NEP}}{\sqrt{\tau/2}}, \quad (4)$$

where the factor of 2 accounts for the conversion between the frequency and time domains. The noise at the detector may in turn be referred to the specific intensity on the sky,

$$\delta I_\nu = \frac{\delta P}{A\Omega \Delta\nu (\alpha\epsilon f)}, \quad (5)$$

where  $\Delta\nu$  is the bandwidth of the synthesized frequency channels. The PIXIE mission concept [18] presents a worked example for the sensitivity improvements possible with existing technology. With etendue  $4 \text{ cm}^2 \text{ sr}$  and maximum phase delay of 1 cm, PIXIE achieves spectral sensitivity for a one-second integration of  $\delta I_\nu = 2.4 \times 10^{-22} \text{ W m}^{-2} \text{ sr}^{-1} \text{ Hz}^{-1}$  within each synthesized frequency channel of width 15 GHz.

The sensitivity for a background-limited FTS depends on the collecting area (etendue), total power absorbed by the detector (optical load), and the number of synthesized frequency channels (detector sampling). Several scaling laws are important:

**Etendue:** Photon noise increases as the square root of the etendue  $A\Omega$  (Eq. 3). However, since the signal increases *linearly* with etendue, the overall sensitivity *improves* as  $(A\Omega)^{1/2}$ . For fixed angular resolution on the sky, the sensitivity improves linearly with the diameter of the beam-forming optics; however, since etendue must be conserved, larger collecting area for the beam-forming optics requires a corresponding increase in the detector area as well. For fixed collecting area, the sensitivity thus scales linearly with the angular resolution on the sky.

**Optical Load:** An FTS is intrinsically broadband. The highest synthesized frequency channel depends on the mirror throw and detector sampling, but the photon noise depends on the total power absorbed from all frequencies within the instrument passband. A scattering filter restricts the instrument passband to limit the noise contribution and prevent signal aliasing from sources at higher frequencies. At mm wavelengths the sky is dominated by the blackbody CMB, with lesser contributions from the far-infrared background, Galactic dust, and Solar System zodiacal emission.

Figure 3 shows the contribution to the photon noise from these sources, as a function of the highest frequency within the instrument passband. Except for bright regions such as the Galactic center, extending the instrument passband from 600 GHz to a few THz increases the noise by less than 20%.

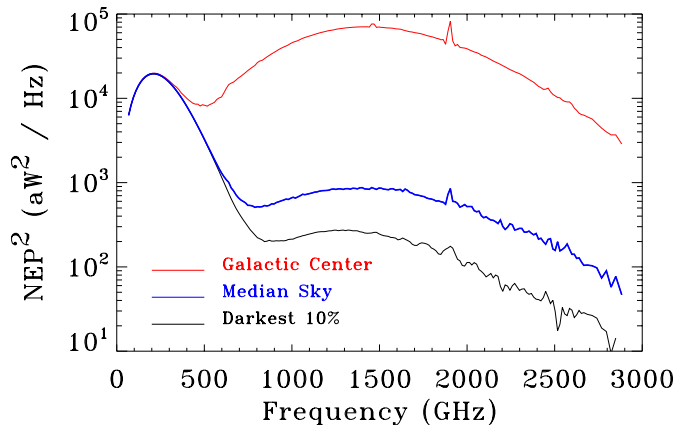


Figure 3: The CMB dominates the photon noise budget. Contributions to the NEP from Galactic dust, zodiacal dust, and the far-IR background are apparent at frequencies above 600 GHz but add less than 20% to the integrated noise.

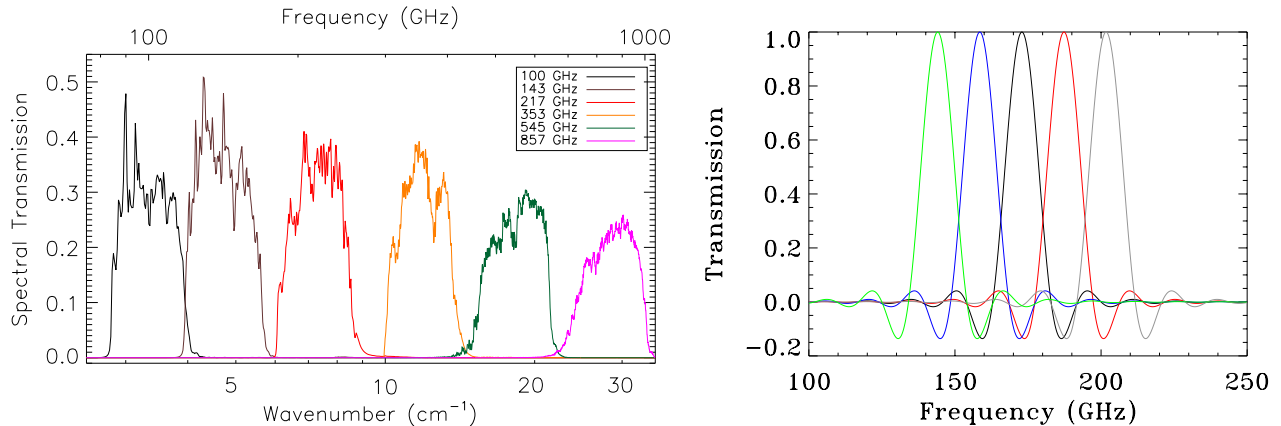


Figure 4: Bandpass filters for a photometer (left) depend on device physics and must be measured to high precision. Synthesized channels for a Fourier transform spectrometer (right) are determined solely by the fringe sampling and apodization and can be determined *a priori*.

**Synthesized Channel Width:** The noise within each frequency channel varies inversely with the synthesized channel width  $\Delta\nu$  (Eq. 5). Although measurements of line emission benefit from relatively narrow channels (to avoid diluting individual lines within broad channels), continuum spectra such as CMB distortions benefit from the broadest channel width consistent with foreground subtraction (§3). Increasing the mirror throw to generate narrower channels provides more but noisier channels within some fixed frequency interval, degrading the overall sensitivity by  $\Delta\nu^{1/2}$  after co-adding channels.

**Synthesized Channel Shape:** Foregrounds from Galactic and extragalactic sources are brighter than CMB spectral distortions (§3). Accurate subtraction of foreground emission requires measurements at multiple frequencies. Errors in the frequency response of individual channels projects foregrounds into the fitted CMB signal, biasing the estimated spectral distortion. Fourier transform spectroscopy offers significant advantages for calibration and foreground subtraction. The frequency response for a conventional photometer is set using physical devices (quasi-optical filters in the optical path, lumped-element circuits, etc). While electromagnetic modeling can predict filter performance to few-percent accuracy, detailed analysis requires supporting measurements of the as-built filter performance. The synthesized channels from Fourier transform spectroscopy, in contrast, depend only on the sampling and apodization of the measured fringe pattern and can be determined *a priori*. The synthesized frequencies may also be set to facilitate foreground subtraction. The central frequency of the  $k^{\text{th}}$  channel is fixed by the maximum phase delay  $Z$ ,  $\nu_k = k(c/Z)$ . To facilitate subtraction of line emission, the maximum phase delay  $Z$  may be chosen to be an integer multiple of the wavelength of the  $J = 1 - 0$  CO line,  $Z = M\lambda_{CO}$ , in which case every  $M^{\text{th}}$  synthesized channel is centered on a CO line.

**Channel Width and Beam Dispersion:** The synthesized channel width is set by the maximum optical phase delay (Eq. 2) and is the same for all channels. As the phase delay mirror moves, the change in the optical path length for a ray along the central axis differs slightly from rays at other angles. As this difference becomes large compared to the wavelength, the fringe contrast (signal amplitude) is diminished when averaged over the beam while the noise is unaffected. The resulting signal loss at the highest desired frequency  $\nu_{\text{max}}$  puts a restriction on the the spectral resolution  $\nu/\Delta\nu$  and the speed of the FTS optics.



A simple rule of thumb is

$$f > \frac{\sqrt{\nu_{\max}/\Delta\nu}}{4} \quad (6)$$

where  $f$  (the optical f-number) is the ratio of diameter to focal length for the FTS transfer mirrors. Since the etendue must be conserved throughout the entire optical system, increasing  $f$  to obtain higher spectral resolution at the maximum frequency requires a corresponding increase in the transfer mirror diameter and mirror-to-mirror spacing (Figure 2). When the size of the FTS exceeds the size of the fore-optics coupling the FTS to the sky, it then drives the size and cost of the observatory.

### 3. Foreground Subtraction

A number of foregrounds contribute appreciable signals at frequencies relevant to CMB spectral distortions. Figure 5 presents an overview. Synchrotron emission, free-free emission, and so-called anomalous microwave emission are the dominant signals at frequencies below  $\sim 70$  GHz [19]. Thermal dust emission from the diffuse interstellar cirrus and the zodiacal dust cloud dominates at high frequencies [20]. Additional foregrounds from the integrated contribution of dust and CO line emission in external galaxies contribute at intermediate frequencies [21, 22]. The combined foreground signal is 2–3 orders of magnitude brighter than CMB spectral distortions and must be subtracted to corresponding accuracy [14, 23].

A number of techniques can be deployed to identify, model, and subtract foreground emission [10, 14, 20, 21, 23, 24]. Parametric models fit multi-frequency data along individual lines of sight to determine parameters specifying the amplitude and frequency dependence of each component. More complex models employ additional information from spatial

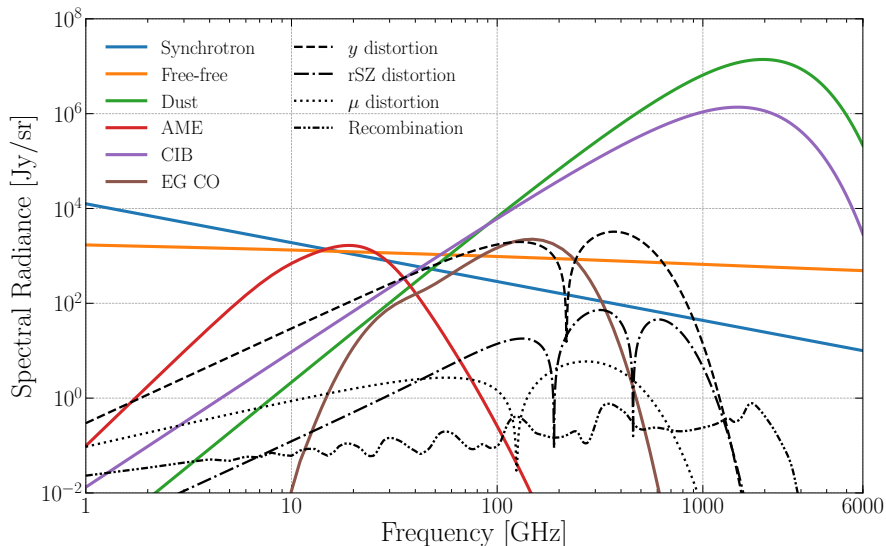


Figure 5: Broadband Galactic and extra-galactic foregrounds lie in the same frequency range as the CMB and its spectral distortions. The Galactic signals include synchrotron (blue), free-free (orange) and anomalous microwave emission (AME, red) at low-frequencies and thermal dust emission (green) at high-frequencies. The cosmic infrared background (CIB, purple) and extra-galactic carbon monoxide integrated over redshift (EG CO, brown) also contribute at mid-to high-frequencies. Zodiacal emission and Galactic molecular lines have been excluded assuming the use of spatial information. The predicted spectral distortion signals are shown in black.



and frequency correlations present in the data to isolate CMB distortions from foreground emission. Ancillary data may also be used to constrain foreground emission, restricting either the spatial distribution or frequency dependence of individual foreground components. Here we use multi-frequency parametric modeling to quantify the impact of foreground emission on sensitivity and identify where additional foreground measurements would be useful [24]. Since we ignore spatial/frequency correlations in the data, the analysis effectively represents a worst-case scenario. The key results of foreground analysis are:

- **Astrophysical foregrounds, not raw sensitivity, are the limiting factor for spectral distortions.** Although the spectral shape of CMB distortions can be calculated to high precision, the frequency dependence of the various foreground components is not known to similar precision and must be determined from the data. If no prior constraints are placed on foreground spectral dependences, foreground modeling degrades the sensitivity to CMB spectral distortions by a factor of 30 compared to the ideal case with no foreground emission. Constraining foregrounds through external priors (e.g. 1% constraints on power-law emission parameters) produces modestly better results. Fully subtracting the foregrounds through parametric models requires constraints at the  $10^{-4}$  level, either through prior knowledge or from a fit of the multifrequency observations of spectrometer data.
- **Data at frequencies below 100 GHz are important to break foreground degeneracies.** Emission from the diffuse dust cirrus and the cosmic infrared background dominates the sky at frequencies above 600 GHz, beyond the Wien cutoff in the CMB spectrum, and are the main foreground contaminants above 100 GHz, where CMB spectral distortions are largest. Data in many frequency channels above 100 GHz, all the way into the THz range, can readily obtain high signal-to-noise measurements on those high-frequency foreground components with sufficient redundancy to validate foreground emission models or refine them if necessary. At lower frequencies, confusion among multiple foreground components (synchrotron, free-free, AME, and extragalactic line emission) overlap with the CMB and require high signal-to-noise ratio data in multiple channels to separate the CMB from the combined foregrounds.

Foreground subtraction methods are rapidly evolving. In addition to multi-frequency parametric models, methods exploiting the spatial structure of foreground components and/or external data sets provide additional handles to separate astrophysical foregrounds from spectral distortion signals. Note that the various foreground components need not be identified and fit individually; rather, CMB spectral distortion science requires only separation of the cosmological signal from the combined foreground emission. Non-parametric models or moment methods [25] are promising and important avenues for continued research.

Additional insight into foreground emission can come from dedicated foreground measurements. The large lever arm between the foreground and CMB distortion amplitudes at both high and low frequencies allows constraints on the foreground spectral energy distribution even at sensitivities unable to directly probe CMB distortions. Measurements at sub-mm wavelengths from balloon platforms can constrain dust properties while data from ground-based or balloon instruments help distinguish the competing low-frequency foregrounds.

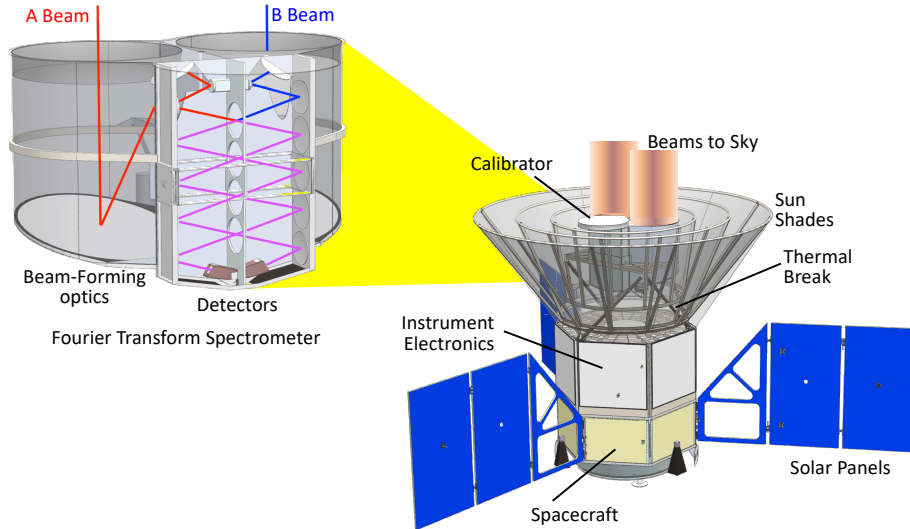


Figure 6: The PIXIE mission concept provides a costed example for a pathfinder spectral distortion mission.

## 4. Mission Concept

Order-of-magnitude improvements over current upper limits require continuous spectra at modest spectral resolution, covering 6 or more octaves in frequency with part-per-million channel-to-channel calibration stability. Such broad frequency coverage precludes ground-based measurements, which are limited to the available atmospheric windows at frequencies below 300 GHz. Balloon missions can play an important role as technology pathfinders, but are limited in integration time and environmental stability. Broad frequency coverage with precision calibration requires a space mission.

A broad-band Fourier transform spectrometer (FTS) to measure CMB spectral distortions has been proposed for several recent opportunities (e.g. PIXIE [18, 26] as a NASA MIDEX mission, as one of the instruments on PRISM [27, 28], an ESA L-class mission, and PRISTINE as an ESA F-class mission). Figure 6 shows the PIXIE mission. It consists of a single cryogenic FTS with a blackbody calibrator capable of moving to block either aperture. A composite hexapod structure provides mechanical support and thermal isolation for the instrument. Nested thermal shields provide passive cooling at 150 K while shielding the instrument against thermal emission from the Sun and warm spacecraft. A mechanical cryocooler provides cooling from 280 K to 4.5 K, with intermediate stages intercepting heat from the hexapod supports at 68 and 17 K. Adiabatic demagnetization refrigerators (ADRs) cool the instrument and detectors. A spacecraft bus provides power, avionics, communication, and propulsion.

The PIXIE observatory would be placed into a Sun-Earth L2 halo orbit and would observe for a projected 4-year mission. Its projected sensitivity would detect the expected  $y$ -distortion (electron pressure) from the growth of structure at 450 standard deviations and the relativistic correction (electron temperature) at  $15\sigma$  to precisely determine the amplitude of baryonic feedback in structure formation. While PIXIE’s raw sensitivity in principle enables a few-standard-deviation detection of the  $\mu$ -distortion from dissipation of primordial density perturbations, astrophysical foregrounds are likely to prevent such a detection (§3).

We outline below a mission concept (Figure 7), based on PIXIE and similar recent concepts, capable of detecting the minimal  $\mu$ -distortion from dissipation of primordial anisotropy even for the worst-case foreground scenario. It consists of several nearly-identical modules, each of which uses a polarizing FTS to measure the signal difference between

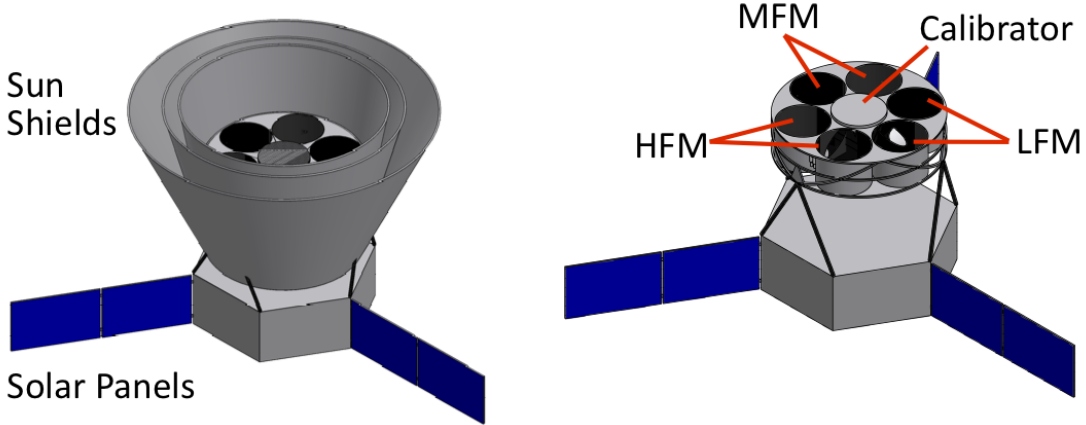


Figure 7: Multiple FTS modules on a common spacecraft bus can be optimized to separate CMB spectral distortions from competing foreground emission. Here 3 modules are shown, although other configurations are possible. The right panel suppresses the sun shields for clarity.

the sky and a blackbody calibrator. As with PIXIE or PRISM, a layered combination of passive (radiative) cooling, mechanical cryocoolers, and sub-K coolers maintains the FTS at a temperature of 2.725 K (isothermal with the CMB) and the detectors at 0.1 K.

The optical passband and maximum phase delay differ for each module so that the white noise level and synthesized frequency bands are optimized for either the CMB distortion signals or the competing foreground emission. A mid-frequency module (MFM) has etendue  $4 \text{ cm}^2 \text{ sr}$ , optical passband 20–600 GHz, and 20 GHz channel width to obtain spectral sensitivity  $\delta I_{MFM} = 1.2 \times 10^{-22} \text{ W m}^{-2} \text{ Hz}^{-1} \text{ sr}^{-1}$  with a 1-second integration. If foregrounds were negligible, the MFM alone could reach the full science goals with a 4-year integration.

Foreground subtraction requires additional sensitivity at both higher and lower frequencies. A high-frequency module (HFM) with etendue  $4 \text{ cm}^2 \text{ sr}$ , optical passband 400–6000 GHz, and 60 GHz channel width has sensitivity  $\delta I_{HFM} = 6.5 \times 10^{-23} \text{ W m}^{-2} \text{ Hz}^{-1} \text{ sr}^{-1}$  to characterize the bright high-frequency foregrounds. The optical passband minimizes photon noise from the CMB while still allowing sufficient overlap with the MFM to cross-calibrate the two modules. Finally, a low-frequency module (LFM) uses etendue  $14 \text{ cm}^2 \text{ sr}$ , optical passband 10–40 GHz, and 2.5 GHz channel width to obtain sensitivity  $\delta I_{LFM} = 2.9 \times 10^{-23} \text{ W m}^{-2} \text{ Hz}^{-1} \text{ sr}^{-1}$  for low-frequency foregrounds. The larger etendue prevents signal attenuation at frequencies below the waveguide cutoff, allowing multi-mode operation down to 10 GHz. By cutting off the optical response at 40 GHz, the LFM again excludes most of the CMB photon noise. Since the LFM optical passband only covers 2 octaves, signal dispersion over the larger phase delay is readily controlled<sup>1</sup>.

Figure 8 shows the predicted performance. A mission with a single module of each type achieves  $|y| < 6.6 \times 10^{-9}$  and  $|\mu| < 5.2 \times 10^{-8}$  (95% CL) within a 4-year mission. A mission with additional modules (4 LFM, 4 MFM, and 1 HFM) achieves limits  $|y| < 3.3 \times 10^{-9}$ ,  $|\mu| < 1.9 \times 10^{-8}$  (95% CL), and could detect the primordial hydrogen and helium recombination lines at  $2\sigma$  within a 10-year mission even for pessimistic foreground assumptions.

Incremental progress is possible, even likely. A “full” mission ( $4 \times 4 \times 1$ ) with no

<sup>1</sup> By comparison, controlling signal dispersion across the MFM’s 6 octaves but with 2.5 GHz channel width would require increasing the MFM transfer mirror diameter by a factor of 64.

foregrounds detects  $\mu$  at  $77\sigma$  (compared to  $2.1\sigma$  with foregrounds). Even a minimal mission such as PIXIE can detect the  $y$  distortion and relativistic correction at high significance, while opening a wide discovery space for new physics through the  $\mu$  distortion. Pathfinders, either from space or balloon platforms, can provide new foreground measurements, directly constraining foreground emission while determining the extent to which spatial/frequency correlations can improve foreground subtraction.

Each module is based entirely on existing technologies; no technology development is required. While no formal cost estimates are available for this concept, full missions using a single instrument module have been proposed. The PIXIE mission has been proposed to NASA’s MIDEX program with cost cap \$250M (FY17) while the PRISM mission (including both a large imager and a smaller spectrometer) has been proposed to ESA’s L-class program. Instrument costs are dominated by the cryogenic cooling, which is common to all modules.

## 5. Conclusions

Simple upgrades to the seminal FIRAS instrument would improve sensitivity by three orders of magnitude or more, providing new tests for the standard cosmology while opening new windows for discovery. No new technologies are required; both the detectors, cryogenics, and instrumentation have been demonstrated.

Detection of CMB spectral distortions is primarily limited by the need to identify and subtract astrophysical foregrounds. As such, new foreground data combined with sustained effort developing methods to identify, model, and subtract foreground emission could significantly reduce the instrument noise levels required to reach specific science goals. Even in a worst-case foreground scenario, much of the science goals could be captured by a single FTS within the cost caps of the NASA MIDEX program. A more ambitious mission using multiple copies of a basic FTS design could reach a fundamental sensitivity threshold to detect the distortions from primordial density perturbations, providing an independent test of inflation on physical scales orders of magnitude beyond any other measurement.

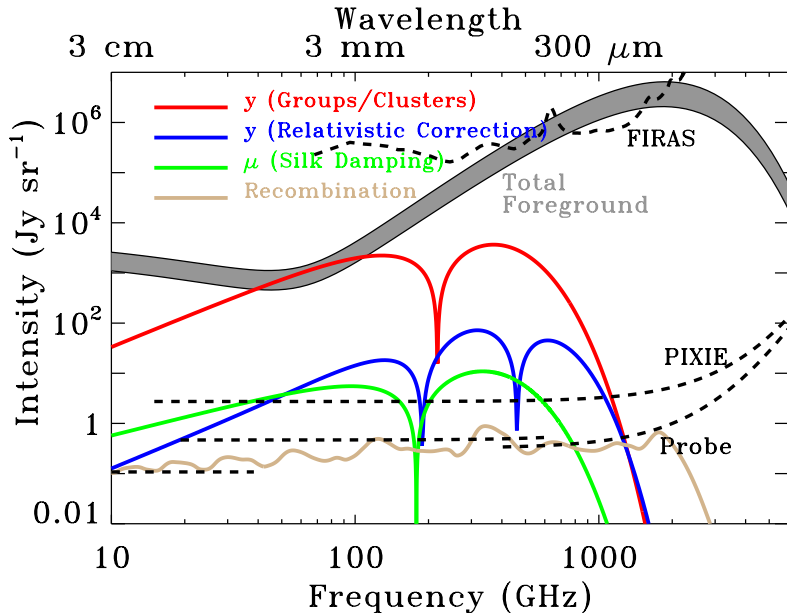


Figure 8: Spectral distortions are observable using current technology even for worst-case foregrounds.

## References

- [1] J. Chluba, A. Kogut, S. P. Patil, M. H. Abitbol, N. Aghanim, Y. Ali-Haïmoud, M. A. Amin, J. Aumont, N. Bartolo, and K. Basu, “Spectral Distortions of the CMB as a Probe of Inflation, Recombination, Structure Formation and Particle Physics,” *BAAS* **51**, p. 184, May 2019.
- [2] Y. B. Zeldovich and R. A. Sunyaev, “The Interaction of Matter and Radiation in a Hot-Model Universe,” *Astrophysics and Space Science* **4**, pp. 301–316, July 1969.
- [3] A. F. Illarionov and R. A. Sunyaev, “Comptonization, the spectrum of RELICT radiation, and the thermal history of the universe,” *Astronomicheskii Zhurnal* **51**, pp. 1162–1176, Dec. 1974.
- [4] J. Chluba and R. A. Sunyaev, “The evolution of CMB spectral distortions in the early Universe,” *Monthly Notices of the Royal Astronomical Society* **419**, pp. 1294–1314, Jan. 2012.
- [5] R. Khatri and R. A. Sunyaev, “Beyond  $y$  and  $\mu$ : the shape of the CMB spectral distortions in the intermediate epoch,  $1.5 \times 10^4 < z < 2 \times 10^5$ ,” *JCAP* **2012**, p. 016, Sep 2012.
- [6] J. Chluba and D. Jeong, “Teasing bits of information out of the CMB energy spectrum,” *Monthly Notices of the Royal Astronomical Society* **438**, pp. 2065–2082, Mar. 2014.
- [7] J. Chluba, “Green’s function of the cosmological thermalization problem - II. Effect of photon injection and constraints,” *Monthly Notices of the Royal Astronomical Society* **454**, pp. 4182–4196, Dec 2015.
- [8] T. R. Slatyer, “Indirect dark matter signatures in the cosmic dark ages. II. Ionization, heating, and photon production from arbitrary energy injections,” *Phys. Rev. D* **93**, p. 023521, Jan 2016.
- [9] S. K. Acharya and R. Khatri, “Rich structure of nonthermal relativistic CMB spectral distortions from high energy particle cascades at redshifts  $z \lesssim 2 \times 10^5$ ,” *Phys. Rev. D* **99**, p. 043520, Feb 2019.
- [10] D. J. Fixsen, E. S. Cheng, J. M. Gales, J. C. Mather, R. A. Shafer, and E. L. Wright, “The Cosmic Microwave Background Spectrum from the Full COBE FIRAS Data Set,” *The Astrophysical Journal* **473**, p. 576, Dec. 1996.
- [11] M. Bersanelli, G. F. Smoot, M. Bensadoun, G. de Amici, M. Limon, and S. Levin, “Measurements of the CMB Spectrum at Centimeter Wavelengths,” *Astrophysical Letters and Communications* **32**, p. 7, Jan 1995.
- [12] S. T. Staggs, N. C. Jarosik, S. S. Meyer, and D. T. Wilkinson, “An Absolute Measurement of the Cosmic Microwave Background Radiation Temperature at 10.7 GHz,” *ApJ* **473**, p. L1, Dec 1996.
- [13] M. Gervasi, M. Zannoni, A. Tartari, G. Boella, and G. Sironi, “TRIS. II. Search for CMB Spectral Distortions at 0.60, 0.82, and 2.5 GHz,” *ApJ* **688**, pp. 24–31, Nov 2008.

- [14] D. J. Fixsen, A. Kogut, S. Levin, M. Limon, P. Lubin, P. Mirel, M. Seiffert, J. Singal, E. Wollack, and T. Villela, “ARCADE 2 Measurement of the Absolute Sky Brightness at 3-90 GHz,” *ApJ* **734**, p. 5, Jun 2011.
- [15] G. Cabass, A. Melchiorri, and E. Pajer, “ $\mu$  distortions or running: A guaranteed discovery from CMB spectrometry,” *Phys. Rev. D* **93**, p. 083515, Apr 2016.
- [16] J. Chluba, “Which spectral distortions does  $\Lambda$ CDM actually predict?,” *Monthly Notices of the Royal Astronomical Society* **460**, pp. 227–239, Jul 2016.
- [17] J. C. Mather, “Bolometer noise: nonequilibrium theory,” *Applied Optics* **21**, pp. 1125–1129, Mar. 1982.
- [18] A. Kogut, D. J. Fixsen, D. T. Chuss, J. Dotson, E. Dwek, M. Halpern, G. F. Hinshaw, S. M. Meyer, S. H. Moseley, M. D. Seiffert, D. N. Spergel, and E. J. Wollack, “The Primordial Inflation Explorer (PIXIE): a nulling polarimeter for cosmic microwave background observations,” *Journal of Cosmology and Astroparticle Physics* **7**, p. 25, July 2011.
- [19] C. L. Bennett, D. Larson, J. L. Weiland, N. Jarosik, G. Hinshaw, N. Odegard, K. M. Smith, R. S. Hill, B. Gold, and M. Halpern, “Nine-year Wilkinson Microwave Anisotropy Probe (WMAP) Observations: Final Maps and Results,” *ApJS* **208**, p. 20, Oct 2013.
- [20] Planck Collaboration, R. Adam, P. A. R. Ade, N. Aghanim, M. I. R. Alves, M. Arnaud, M. Ashdown, J. Aumont, C. Baccigalupi, and A. J. Banday, “Planck 2015 results. X. Diffuse component separation: Foreground maps,” *A&A* **594**, p. A10, Sep 2016.
- [21] Planck Collaboration, P. A. R. Ade, N. Aghanim, C. Armitage-Caplan, M. Arnaud, M. Ashdown, F. Atrio-Barandela, J. Aumont, C. Baccigalupi, and A. J. Banday, “Planck 2013 results. XXX. Cosmic infrared background measurements and implications for star formation,” *A&A* **571**, p. A30, Nov 2014.
- [22] N. Mashian, A. Loeb, and A. Sternberg, “Spectral distortion of the CMB by the cumulative CO emission from galaxies throughout cosmic history,” *Monthly Notices of the Royal Astronomical Society* **458**, pp. L99–L103, May 2016.
- [23] D. J. Fixsen, “The Temperature of the Cosmic Microwave Background,” *ApJ* **707**, pp. 916–920, Dec 2009.
- [24] M. H. Abitbol, J. Chluba, J. C. Hill, and B. R. Johnson, “Prospects for measuring cosmic microwave background spectral distortions in the presence of foregrounds,” *Monthly Notices of the Royal Astronomical Society* **471**, pp. 1126–1140, Oct 2017.
- [25] J. Chluba, J. C. Hill, and M. H. Abitbol, “Rethinking CMB foregrounds: systematic extension of foreground parametrizations,” *Monthly Notices of the Royal Astronomical Society* **472**, pp. 1195–1213, Nov 2017.
- [26] A. Kogut, J. Chluba, D. J. Fixsen, S. Meyer, and D. Spergel, “The Primordial Inflation Explorer (PIXIE),” in *Space Telescopes and Instrumentation 2016: Optical, Infrared, and Millimeter Wave*, Society of Photo-Optical Instrumentation Engineers (SPIE) Conference Series **9904**, p. 99040W, Jul 2016.

- [27] PRISM Collaboration, P. Andre, C. Baccigalupi, D. Barbosa, J. Bartlett, N. Bartolo, E. Battistelli, R. Battye, G. Bendo, and J.-P. Bernard, “PRISM (Polarized Radiation Imaging and Spectroscopy Mission): A White Paper on the Ultimate Polarimetric Spectro-Imaging of the Microwave and Far-Infrared Sky,” *arXiv e-prints*, p. arXiv:1306.2259, Jun 2013.
- [28] P. André, C. Baccigalupi, A. Banday, D. Barbosa, B. Barreiro, J. Bartlett, N. Bartolo, E. Battistelli, R. Battye, and G. Bendo, “PRISM (Polarized Radiation Imaging and Spectroscopy Mission): an extended white paper,” *Journal of Cosmology and Astro-Particle Physics* **2014**, p. 006, Feb 2014.